Chemosphere 393 (2025) 144775

Contents lists available at ScienceDirect

Chemosphere

journal homepage: www.elsevier.com/locate/chemosphere

Crop straw biochar enhances hydrocarbon adsorption in ground water

Abhijeet Pathy [a,b], M. Anne Naeth [a,b,*], Scott X. Chang [a,b]

[a] Department of Renewable Resources, University of Alberta, Canada
[b] Land Reclamation International Graduate School, University of Alberta, Canada

HIGHLIGHTS

- Comprehensive simultaneous adsorption of 12 hydrocarbons in actual ground water matrix.
- Hydrocarbon concentrations reduced >40 % within the first minute of biochar addition.
- Remediation efficiency >99 % for some petroleum hydrocarbons with biochar at 2 g L^{-1}
- Adsorption via chemisorption and diffusion with multilayered heterogeneous binding.
- Functional groups enable hydrocarbon adsorption via π-π and hydrophobic bonds.

GRAPHICAL ABSTRACT

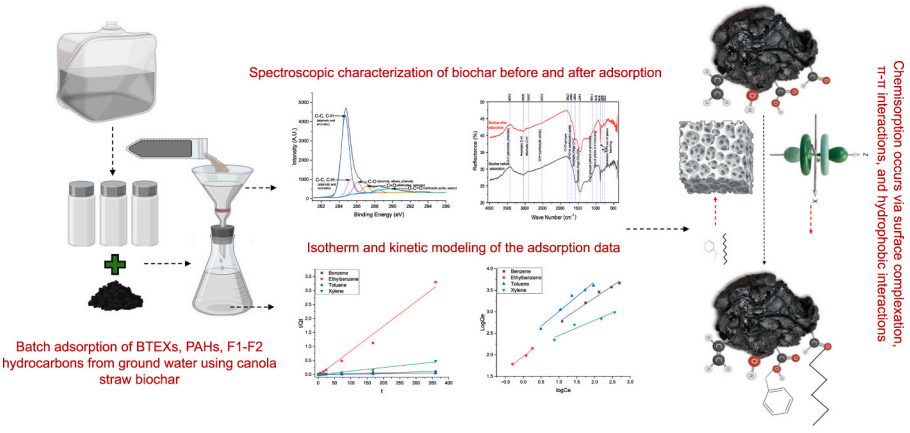

ARTICLE INFO

Handling editor: Yongmei Li

Keywords:
Biochar
Ground water
Petroleum hydrocarbons
BTEX
PAH
Adsorption
Remediation

ABSTRACT

Hydrocarbon fuel production and use can pose environmental risks, such as spills during extraction and transportation, which can contaminate soil, damage vegetation, adversely affect human and animal health, and contaminate ground water with soluble hydrocarbons, that could spread to surrounding areas. Our study evaluates the simultaneous adsorption capacity of canola straw biochar for 12 hydrocarbon pollutants in ground water from a northern peatland. This approach simulates the simultaneous contamination of multiple hydrocarbon classes in a complex aqueous matrix. In the laboratory, canola straw biochar remediated benzene, toluene, ethylbenzene, and xylene (BTEX), and linear chained and polycyclic aromatic hydrocarbons from ground water. BTEX concentrations significantly decreased with application of 1 g L^{-1} biochar, achieving a remediation efficiency of over 95 % within 7 days. Increasing application rates enhanced remediation efficiency, exceeding 99 % at a 2 g L^{-1} application rate. Hydrocarbon adsorption on biochar is a complex process involving surface interactions and diffusion-controlled steps, with the kinetic data fitting well to models indicative of chemisorption. X-ray photoelectron spectroscopy, BET/CO_2 porosimetry and Fourier transform infrared spectroscopy corroborated theoretical isotherm and kinetic models, indicating that functional groups on the biochar surface play a crucial role in adsorption, primarily through hydrophobic and π-π interactions. The results enhanced our understanding of adsorption mechanisms for multiple hydrocarbon classes in complex matrices

* Corresponding author. Land Reclamation and Restoration Ecology; Department of Renewable Resources, Faculty of Agricultural, Life and Environmental Sciences, University of Alberta; 855C General Services Building, Edmonton, Alberta, Canada, T6G 2H1.
E-mail addresses: pathy@ualberta.ca (A. Pathy), anaeth@ualberta.ca (M.A. Naeth).

https://doi.org/10.1016/j.chemosphere.2025.144775
Received 11 August 2025; Received in revised form 14 November 2025; Accepted 15 November 2025
Available online 25 November 2025

under controlled laboratory conditions, and positioned canola straw biochar as an effective remediation technique for hydrocarbon water treatment. Biochar is made from waste agricultural materials and sequesters carbon, contributing to environmentally sustainable remediation and a circular economy.

1. Introduction

The economic prosperity of the 21st century is supported by energy consumption, and current trends indicate no signs of deceleration. Despite enthusiasm and efforts to transition to cleaner, renewable energy sources, oil remains a significant contributor to meeting current energy demands, with global oil production in 2021 at 4.423 billion tons (Zhang et al., 2024). During exploration, extraction, transportation, and storage processes, oil can be spilled, resulting in oil-contaminated water. The International Tanker Owners Pollution Federation Limited database estimates that approximately 2000 tons of oil was spilled in 2023, resulting in contamination by petroleum hydrocarbons (PHCs). This database only reports large (>700 tonnes) or medium (7–700 tonnes) oil spills; hence, these data likely underestimate the total oil lost (Oil Tanker Spill Statistics, 2023). PHC contamination spreads through wind, water, and sediment, impacting many oil-producing regions worldwide, including the Middle East, North America, Russia, Africa, Europe, and Asia-Pacific. This leads to significant ecological damage to land, beaches, and wetlands (Alexandersson and Klevebring, 2019).

When petroleum hydrocarbons enter the environment, they undergo weathering, including processes such as dispersion, evaporation, dissolution, sorption, and biodegradation, epending on their properties and environmental conditions (Logeshwaran et al., 2018). PHCs migrate vertically and laterally into ground water after soil contamination. During this movement, smaller hydrocarbons are weathered and may evaporate, while others undergo processes such as dissolution, dispersion, and biodegradation (Gill et al., 2024). These processes facilitate the movement of petroleum hydrocarbons from the surface or subsurface into ground water, leading to contamination. PHCs consist of a wide variety of compounds derived from crude oil or natural gases, including alkanes, cycloalkanes, aromatics, alkenes, dienes, alkynes, polycyclic aromatic hydrocarbons (PAHs), asphaltenes, and resins (Speight, 2006). F1 hydrocarbons comprise aliphatics with carbon numbers from C_6 to C_{10} (molecular weight 86–142 g/mol), representing lighter, more volatile compounds. The F2 hydrocarbons include aliphatics from C_{10} to C_{16} (molecular weight 142–226 g/mol). The F3 hydrocarbons include C_{16} to C_{34}, and the F4 hydrocarbons include C_{34} to C_{50}. The contaminants of primary concern in an aqueous system are the mobile and highly water-soluble fractions (F1, F2). Only a few of these chemical compounds have been well characterized for toxicological effects. The toxicity of individual contaminants depends on their chemical nature, mode, concentration, and duration of exposure. PHCs can cause serious health problems in animals and humans (Wang et al., 2017; Ambaye et al., 2022), and can inhibit vegetation, leading to stunted plant growth, deformed plant parts, and declining resistance to disease and pests (Mohanta et al., 2024). Thus, it is essential to remediate PHCs from affected environments, and various regulatory organizations worldwide mandate remediation to safeguard human and animal lives and protect ecosystem functions, biodiversity, and soil and water quality (Kuppusamy et al., 2020).

Several methods have been employed to remediate PHCs, including pump and treat, air sparging, bioremediation, chemical oxidation, permeable reactive barriers, monitored natural attenuation, and phytoremediation (Kakkar et al., 2023). The choice of remediation techniques needs to be based on efficiency, economic feasibility, and environmental sustainability. Biochar can be a proven, effective remediation technique for various organic and inorganic contaminants and has the potential to become a cost-effective remediation approach (Mohan et al., 2014).

The thermochemical decomposition of biomass in the absence of oxygen produces biochar, a carbon-rich product. Due to its stability, biochar is valued for waste management and carbon sequestration, aiding climate change mitigation (Gupta et al., 2020). Biochar can be produced from inexpensive raw materials such as agricultural, animal, forest, and municipal waste, making it a potentially cost-effective adsorbent. Biochar properties can vary significantly depending on the biomass and production conditions (Ghodake et al., 2021). The production temperature range is used to optimize the balance of surface area, pore development, and surface chemistry. Biochar produced at 450–500 °C typically has higher aromaticity, increased microporosity and mesoporosity, and moderate retention of oxygen-containing functional groups (carboxyl and hydroxyl), relative to lower or higher temperature biochars (Zhang et al., 2022). The feedstock source should be readily available, low-cost, and with proven remediation potential. For example, in regions such as Alberta, canola straw waste offers a practical, local feedstock, minimizing transport costs and supporting efficient remediation of sites prone to PHCs contamination.

Recent research demonstrated biochar's effectiveness in removing petroleum hydrocarbons, with laboratory studies reporting removal efficiencies exceeding 90 % for BTEX and PAHs via π-π interactions, hydrophobic partitioning, and pore-filling mechanisms (Gurav et al., 2021; Mohammadi et al., 2020; Sun et al., 2022). However, most studies focus on single contaminants in synthetic solutions, failing to capture competitive adsorption dynamics in real ground water containing multiple hydrocarbon classes simultaneously (Dong et al., 2023; Fang et al., 2025). Despite these advances, critical knowledge gaps limit biochar's widespread application for PHC remediation in ground water. Most biochar studies have examined single contaminants, such as specific PAHs or BTEX compounds. However, petroleum-contaminated ground water contains multiple hydrocarbon classes, including BTEX, linear-chain aliphatics (F1–F4), and PAHs, that coexist and compete for adsorption sites. Few studies have investigated the simultaneous removal of these diverse contaminant groups, leaving competitive adsorption dynamics poorly understood (Ossai et al., 2020). Although most laboratory studies test adsorption in pure water, real environments, such as ground water or industrial wastewater, contain diverse ions and other constituents that affect adsorption outcomes. Thus, field and laboratory results often differ, highlighting the need to use more realistic matrices in research for meaningful application. (Gurav et al., 2021). Further research is needed to better understand the mechanisms underlying PHC adsorption on biochar, which would enhance its effectiveness and applicability in remediation. This study aims to address these research gaps by using biochar to simultaneously remediate different groups of PHCs in ground water.

This study has two key objectives. (1) To evaluate the remediation potential of canola straw biochar for simultaneous removal of petroleum hydrocarbons from ground water; specifically BTEX, PAHs, and F1 and F2 aliphatic hydrocarbons, from ground water, while assessing the effect of biochar dosage on remediation efficiency. To ensure field relevance, actual ground water containing naturally occurring ions and compounds was used, along with a multi-contaminant source (crude oil), to better approximate the chemical complexity of contaminated sites than studies using synthetic solutions. (2) To develop a comprehensive understanding of petroleum hydrocarbon adsorption mechanisms by fitting experimental data to various kinetic and isotherm models and validating these theoretical findings using advanced analytical techniques.

The novelty of this research lies in two key contributions. (1) This is the first study to evaluate biochar's ability to simultaneously remove twelve petroleum hydrocarbons spanning BTEX, PAHs, and F1 and F2 aliphatic fractions from real ground water, addressing the critical gap in

understanding competitive adsorption dynamics in complex environmental matrices. (2) Comprehensive mechanistic insights are provided through advanced characterization techniques (XPS, FTIR, BET/CO_2 porosimetry) integrated with kinetic and isotherm modeling. This work advances our understanding of biochar-mediated hydrocarbon remediation mechanisms and addresses the need for further research to enable field-scale biochar applications.

2. Materials and methods

2.1. Ground water collection and spiking with crude oil

For this study, the ground water was collected from a borewell at the Kehew Valve Station near Cold Lake, Alberta, Canada. Before sampling, the water level in the borewell was measured using a water level meter, indicating a depth of 1.72 m. Prior to sampling, five borehole volumes were purged to ensure stagnant water was removed and samples represented actual aquifer conditions. Through siphoning, 90 L of ground water were collected in pails and transported to a laboratory at the University of Alberta, Canada. All the water from the pails was put into one container and mixed together. Three samples were taken from this mixture and assessed for PHCs, including PAHs, BTEX, and F1–F4 hydrocarbons, because of the site's history of crude oil spills. The heavier compounds (F3, F4) have low aqueous solubility and low mobility, indicating they do not pose a dominant threat to the transport mechanisms evaluated in this water-based system. Since only the lighter, more water-soluble fractions of crude oil partition into ground water under field conditions, the crude oil was analyzed only for its volatile hydrocarbon fraction (Table S6).

Samples for BTEX, F1–F4, and PAHs analysis were preserved according to standard protocols and stored at 4 °C prior to analysis by an accredited laboratory (ISO/IEC 17025). BTEX compounds and F1 hydrocarbons were measured using headspace extraction with analytical detection by gas chromatography coupled to flame ionization detection (GC-FID) or mass spectrometry (GC-MS), calibrated with certified standards, following Canadian Council of Ministers of the Environment (CCME) CWS and United States Environmental Protection Agency (USEPA) 8260d modified methods (USEPA, 1996a; CCME, 2008). For F2–F4 hydrocarbons, samples underwent solvent extraction followed by silica gel cleanup to remove polar matrix components, and quantification was performed by GC-FID according to the CCME PHC-CWS modified methods CCME, 2008). PAHs were analyzed using liquid-liquid extraction with dichloromethane via separatory funnel (EPA Method 3510C), followed by concentration and quantification by GC-MS (EPA Method 8270E modified) (USEPA, 1996b; USEPA, 2018). Method validation included matrix spikes, blanks, and duplicates for each sample batch, with all data reviewed for accuracy under ISO/IEC 17025 accreditation protocols. Ground water quality was analyzed for organic and inorganic parameters. Dissolved metals were quantified using ICP-MS and atomic absorption techniques. Anions such as nitrates and chlorides were measured by ion chromatography. Biological oxygen demand and chemical oxygen demand were determined by standard titration methods. Alkalinity and hardness were assessed through titration with standardized reagents. The pH and conductivity measurements were taken using calibrated digital meters.

All analyses followed accredited protocols by the CCME with quality control via blanks, duplicates, and certified standards to ensure data reliability (CCME, 2008). The PHCs found in the ground water were below the limits set by the CCME (CCME, 2008). Therefore, the ground water was spiked with crude oil in the laboratory. The details on ground water characterization, spiking, and corresponding results are provided in the supplementary material.

2.2. Production and characterization of adsorbent

Canola straw biochar was used for the adsorption experiment due to its abundant availability and past performance. Canola straw biochar was effective in the remediation of inorganic contaminants, such as heavy metals, from water (Islam et al., 2021). The canola straw feedstock was sourced from local agricultural producers in Alberta, Canada, and biochar production was produced by InnoTech Alberta (Edmonton, AB, Canada). After air-drying, the feedstocks were converted to biochar via pyrolysis at temperatures from 450 to 500 °C in an oxygen-limited, nitrogen-purged environment.

To understand the surface area and porosity of the biochar, it was characterized by N_2 adsorption-desorption isotherms at 77 K and CO_2 adsorption at 273 K using a Quantachrome Autosorb iQ. N_2 isotherms (0.01–0.99 P/P_0) were analyzed by the multi-point BET method, DFT slit-pore model, and BJH adsorption to determine surface area, pore volume, and size distribution. CO_2 isotherms (0.01–1.0 P/P_0) were processed by DFT to assess ultra-microporosity. Two characterizations were performed to determine the chemical properties of biochar and its influence on adsorption. X-ray photoelectron spectroscopy (XPS) was employed to analyze the surface chemistry and elemental composition. The measurements were performed using a Kratos AXIS Ultra XPS imaging spectrometer. For XPS analysis, a hemispherical electron energy analyzer and a single colour Al K ± X-ray source (1486.6 eV) were used. The binding energies were calibrated using the C 1s peak at 284.8 eV as a reference. Data analyses were performed using CasaXPS software to deconvolute peaks and identify the chemical state of surface elements on the biochar.

The functional groups on the biochar were analyzed using Fourier transform infrared spectroscopy (FTIR). The diffuse reflection (DRIFT) mode was utilized to obtain high-quality spectra from the powdered samples. The FTIR analysis was performed using a Bruker Tensor 27 FTIR spectrometer equipped with a DRIFT accessory. Approximately 20 mg of biochar sample was mixed with 100 mg of potassium bromide (KBr) powder and placed in the DRIFT sample holder. The spectra were collected over the 4000-400 cm^{-1} range with a resolution of 4 cm^{-1}. The collected spectra were analyzed to compare the peaks with corresponding functional groups. Both analyses were performed before and after the adsorption reaction was complete, to determine changes in the surface functional properties of the biochar and their potential relationship with PHC adsorption.

2.3. Adsorption experiments

Batch experiments were performed at room temperature (approximately 22 °C) using the canola straw biochar adsorbent. Kinetics studies were performed with reaction times of 1, 15, and 30 min, and 1, 2, 3, 4, 6, 8, 16, 24, 72, 168, and 360 h after addition of the biochar. The spiked ground water was diluted to five concentrations (100, 80, 60, 40, 20 % of the original spiked solution) with distilled water (see Table S6 for composition of the 100 % spiked solution) and subsequently used in adsorption isotherm experiments. For both experiments, 0.2 g of biochar was weighed into a 200 mL plastic container, and 200 mL of the ground water solution was added to it. Varying dosages (0.5, 1, 2 g L^{-1}) of canola straw biochar were added to ground water samples containing PHCs. After adding the biochar and ground water, the plastic containers were capped and placed on a mechanical orbital shaker operated at 50 rpm for 14 reaction times and 168 h for isotherm and dosage experiments, respectively.

The isotherm and dosage experiments were conducted at 168 h based on preliminary kinetics data showing that equilibrium was reached for most hydrocarbon species within this period, and to ensure comparability between multiple treatments within a feasible experimental timeframe. Control samples consisting of spiked ground water without biochar were run for the entire duration under identical conditions (50 rpm shaking, same temperature, headspace <5 mL, identical sampling intervals). These controls were sampled at 1 min, 24 h, 168 h, and 360 h alongside the biochar-treated samples to quantify any loss of hydrocarbons due to volatilization or other abiotic processes. Additional

controls included biochar with distilled water blanks to analyze any PAHs leaching from the biochar surface. All experiments were conducted with three replicates for quality control.

After the adsorption experiments, biochar was filtered and separated from the ground water, which was then transferred to two vials (40 mL each) and an amber container (100 mL), both preserved with sodium bisulfate. Ground water was analyzed for PAHs by separatory funnel liquid extraction and gas chromatography mass spectrometry (GC/MS) (EPA 3510C/8270E m) (US Environmental Protection Agency, 2018a, 1996b). BTEX and F1 were analyzed by gas chromatography mass spectrometry with a flame ionization detector for headspace analysis. The Canada-wide standards for PHCs were followed for F2–F4 analysis, using hexane/acetone in a Soxhlet extraction and gas chromatograph with the silica gel cleanup method (CCME PHCs-CWS) (CCME, 2008, 2016).

Following the analysis, the removal efficiency and adsorption capacity of the biochar were calculated using Eqs. (1) and (2):

$$\text{Adsorption Capacity} = ((\text{Ci}_{-}\text{ce}) \div \text{W}) \times \text{V} \quad (1)$$

$$\text{Removal Efficiency} = ((\text{Ci}_{-}\text{ce}) \div \text{Ci}) \times 100 \quad (2)$$

Where C_i and C_e are the initial and equilibrium concentrations of various PHCs present in the solution (ppb), W is the weight of biochar added (g), and V is the total volume (mL) of the solution used in the adsorption experiment.

2.4. Isotherm and kinetics

The adsorption of various PHCs onto biochar was assessed to understand the sorption mechanism using various kinetic and isotherm models. The details of the isotherm and kinetic models implemented in this study are provided in the supplementary materials (Tables S1 and S2).

3. Results and discussion

3.1. Biochar as an effective adsorbent for hydrocarbon remediation from ground water

Across all tested reaction times, adsorption onto biochar resulted in a significant decrease in F1 hydrocarbons in ground water treated with biochar. Upon adding biochar (1 min reaction time), F1 concentrations decreased from 11,667 μg L^{-1} to 6567 μg L^{-1}. The concentration of F1 hydrocarbons continued to decrease, reaching a concentration of 383 μg L^{-1} after 360 h, with a removal efficiency of 95 % (Fig. 1a). Similarly, biochar demonstrated high effectiveness in adsorbing F2 hydrocarbons. After biochar application, the F2 hydrocarbons decreased by more than 50 %, and within 24 h fell below the detection limit, indicating a remediation efficiency of nearly 100 (Fig. 1b).

Biochar's overall performance for the adsorption of BTEX compounds was considered highly efficient and effective (Fig. 1c–f). The addition of biochar significantly reduced benzene concentrations. Benzene concentrations dropped from 2500 μg L^{-1} to 900 μg L^{-1} within the first 24 h, then steadily decreased to 200 μg L^{-1} over the following 14 days. The remediation efficiency steadily increased from 41 % at the start of the experiments (1 min of reaction time) to 94 % after 15 days. Ethylbenzene concentrations dropped significantly from 187 μg L^{-1} to 100 μg L^{-1} 1 min after biochar addition, and the trend continued to 1 μg L^{-1} by the end of day 15, demonstrating a 99 % removal efficiency with biochar application. Toluene concentrations decreased from 4000 μg L^{-1} to 2233 μg L^{-1} within 1 min of biochar addition. A rapid decline within the subsequent 24 h reduced toluene concentrations to 327 μg L^{-1}. Over the following 14 days, toluene concentrations continued to decrease, reaching 52 μg L^{-1}, with 98 % removal efficiency. Biochar reduced the xylene concentration in ground water from 1367 μg L^{-1} to 803 μg L^{-1} within the first minute of reaction, with a significant decline to 53 μg L^{-1} within 24 h. The removal efficiency of biochar increased from 41 % at the start of the reaction to 95 % after 24 h of adsorption,

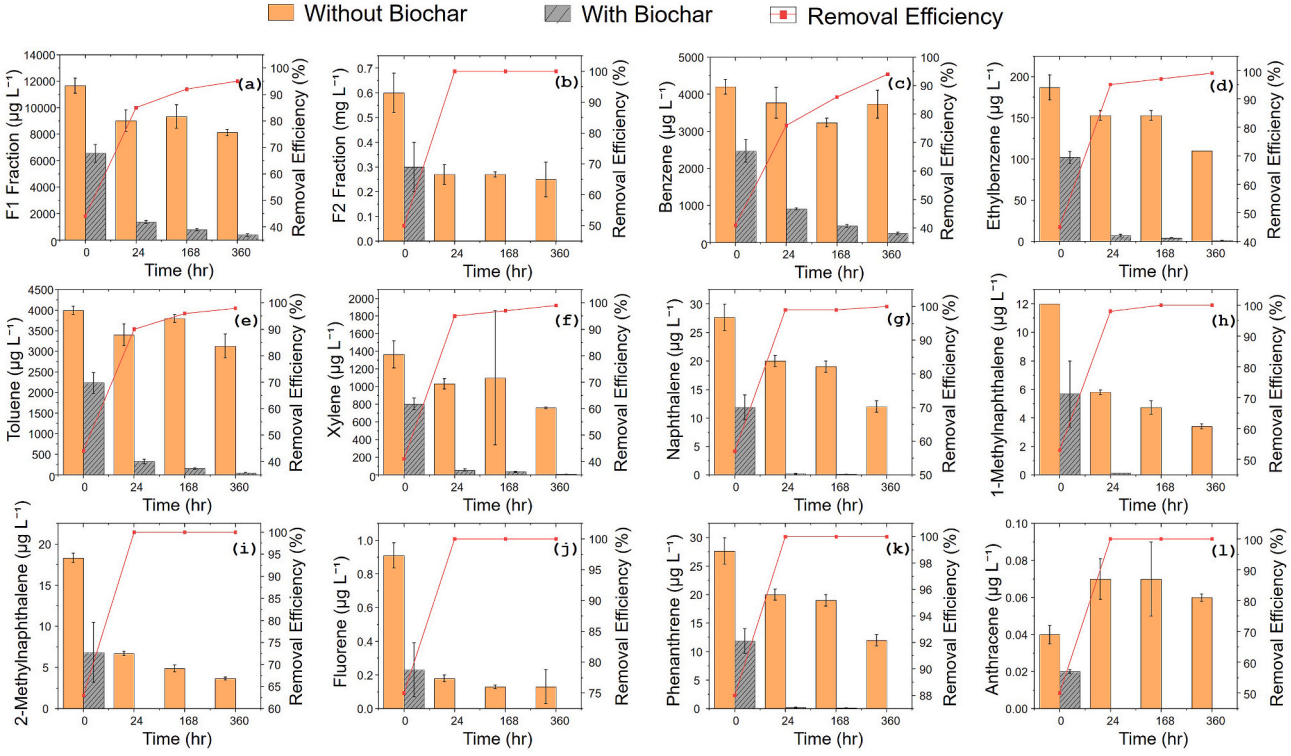

Fig. 1. Removal efficiency and concentration of petroleum hydrocarbons in ground water with and without canola straw biochar. Comparative analysis of (a) F1, (b) F2, (c) benzene, (d) ethylbenzene, (e) toluene, (f) xylene, (g) naphthalene, (h) 1-Methylnaphthalene, (i) 2-Methylnaphthalene, (j) fluorene, (k) phenanthrene, and (l) anthracene.

and rose to 99 % by the end of day 15.

The adsorption performance of biochar for PAHs was highly effective. Unlike BTEX compounds, PAH concentrations were relatively low; hence, for most PAHs, complete adsorption was observed within a short period after adding biochar. For example, 24 h after adding biochar to ground water, concentrations of acridine, anthracene, fluorene, 2-methylnaphthalene, and phenanthrene fell below the detection limit. For naphthalene and 1-methylnaphthalene, complete adsorption took more than 24 h 1-methyl naphthalene concentrations decreased from 12 μg L^{-1} to 5.67 μg L^{-1} following biochar addition, declining significantly within 24 h to 0.11 μg L^{-1}, then to below the detection limit on day 7. Similarly, naphthalene concentrations decreased from 27.67 μg L^{-1} to 11.87 μg L^{-1} following biochar addition, declined significantly within 24 h to 0.19 μg L^{-1}, then decreased over 14 days to below the detection limit of 0.10 μg L^{-1}.

It is noteworthy that, for most PAHs (except anthracene), control samples showed a steady decline over time; however, adding biochar achieved very high adsorption efficiency within a short time. In the control experiments conducted without biochar, the loss of BTEX compounds due to abiotic factors over the 360-h period was modest, with benzene and toluene showing less than 22 % reduction, and ethylbenzene and xylene decreasing by 41–44 %. Reductions in F1 and F2 hydrocarbons were limited to 30–58 %, while PAHs such as 1-MNAP, 2-MNAP, and NAP showed higher natural losses of 57–80 %. In contrast, biochar treatment resulted in a much greater removal across all compounds, with reductions exceeding 90 % for BTEX, over 94 % for F1 and F2 hydrocarbons, and complete (100 %) removal of PAHs, confirming that adsorption to biochar was the dominant mechanism driving pollutant reduction.

From the FTIR analysis, many distinct peaks were identified in the biochar, which corresponded to specific functional groups and their associated vibrational modes (Fig. 2). Biochar has abundant functional groups on its surface, including alcohols, phenols, aromatic C, aliphatic C, carboxylic acids, ethers, and aromatic C═C bonds. Spectral intensity changes in functional groups following adsorption indicate their participation in adsorption via hydrogen bonding and hydrophobic interactions, depending on the nature of the functional groups on the biochar surface. Out-of-plane C–H bending was observed at 978 cm^{-1} before adsorption and was absent in the biochar sample after adsorption. Strong and sharp out-of-plane bending vibrations of aromatic C–H were detected at 876 cm^{-1}, with weaker, narrow peaks at 825 cm^{-1} and 755 cm^{-1}. The peak intensity at 1457 and 876 cm^{-1} was higher for biochar after adsorption.

The intensity changes in these peaks indicate the involvement of aromatic C in the adsorption process. Biochar has graphitic aromatic structures that facilitate hydrophobic interactions with PHC molecules and the thedsorption of aromatic compounds (Guo and Rockstraw, 2007). The aromatic C═C rings, along with the aromatic ring vibration and C–H deformation (observed in FTIR analysis), strongly confirm the material's aromatic structure, which can also enhance π-π interactions (Xue et al., 2012). Consistent with this observation, results from the XPS analysis show the disappearance of the π-π* satellite peak (biochar sample after adsorption) at 293 eV, which confirms the involvement of π-π bonding in the adsorption of PHCs on biochar (Fig. 3a–b). The non-polar fractions of PHCs, such as aliphatic hydrocarbons, BTEX compounds, and PAHs, get adsorbed onto the biochar surface through van der Waals forces, π-π interactions, and hydrophobic interactions. The FTIR and XPS analyses provide evidence of the presence of suitable functional groups on the biochar's surface and their involvement in adsorbing the PHCs.

3.2. *Impact of biochar dosage on hydrocarbon remediation: enhanced F1 and BTEX removal, limited effect on PAHs and F2*

For most PHCs, increasing biochar dosage improved adsorption (Fig. 4), especially at very high concentrations. For all the PHCs under consideration, a removal efficiency of more than 97 % was achieved with a biochar dosage of 2 mg mL^{-1}. For example, the removal efficiency of F1 hydrocarbons increased from 76 to 91 % as the biochar dosage increased from 0.5 to 1 mg mL^{-1} (Fig. 4a); it reached 98 % at 2 mg mL^{-1}. Remediation of F2 hydrocarbons was independent of biochar dosage, as a 0.5 mg mL^{-1} dose was sufficient to completely remediate F2 hydrocarbons from ground water.

The impact of dosage was prominently observed for BTEX compounds. Benzene remediation efficiency increased from 66 to 86 % when the dosage was increased from 0.5 to 1 mg mL^{-1}, and removal efficiency reached 97 % when the dosage was increased to 2 mg mL^{-1} (Fig. 4b). Ethylbenzene showed a similar trend in removal efficiency, increasing from 91 to 99.5 % as the biochar dosage increased from 0.5 to 2 mg mL^{-1} (Fig. 4c). Toluene also responded to biochar dosage; removal efficiency increased from 86 to 95 % when the dosage was increased from 0.5 to 1 mg mL^{-1}, and was almost completely removed (99.4 %) when

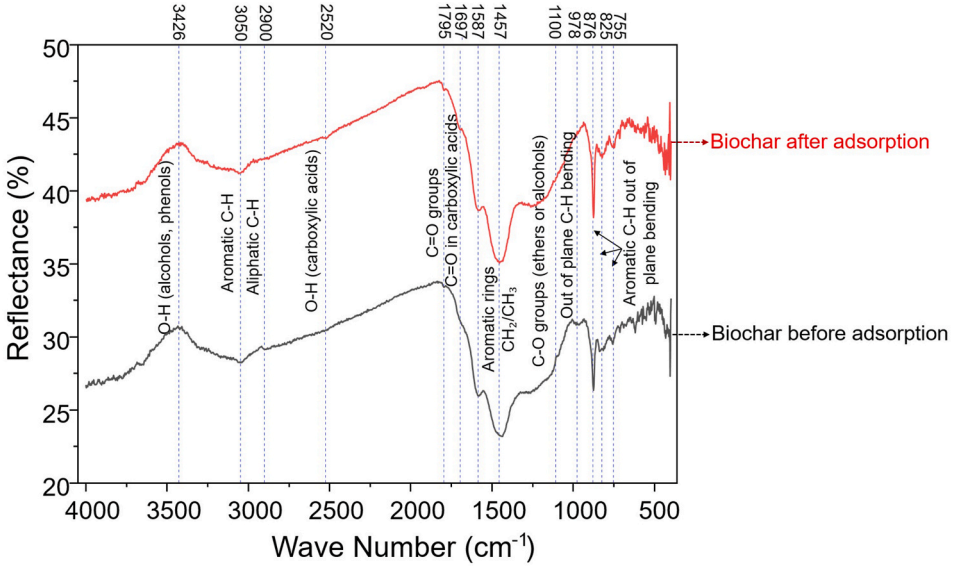

Fig. 2. Fourier transform infrared spectroscopy spectral characterization of biochar: analysis of functional group changes before and after petroleum hydrocarbon adsorption.

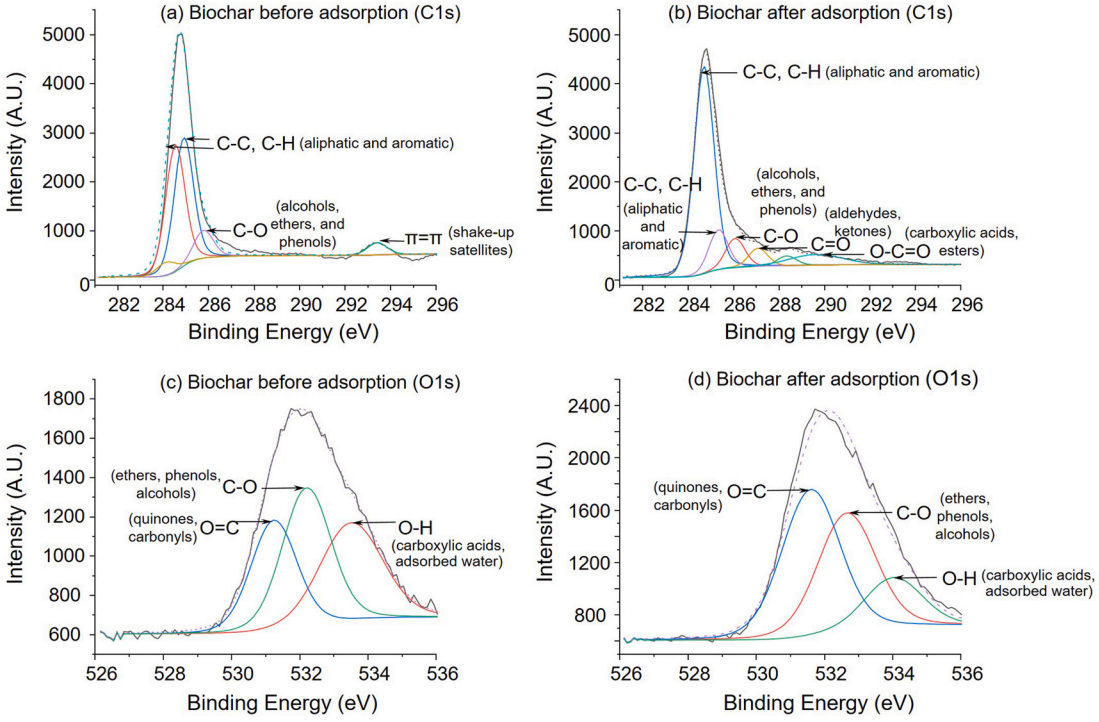

Fig. 3. High resolution X-ray photoelectron spectroscopy spectra of C1s and O1s regions of biochar. Surface chemistry changes before and after petroleum hydrocarbon adsorption, a) C1s spectra for biochar before adsorption, b) C1s spectra for biochar after adsorption, c) O1s spectra for biochar before adsorption, d) O1s spectra for biochar after adsorption.

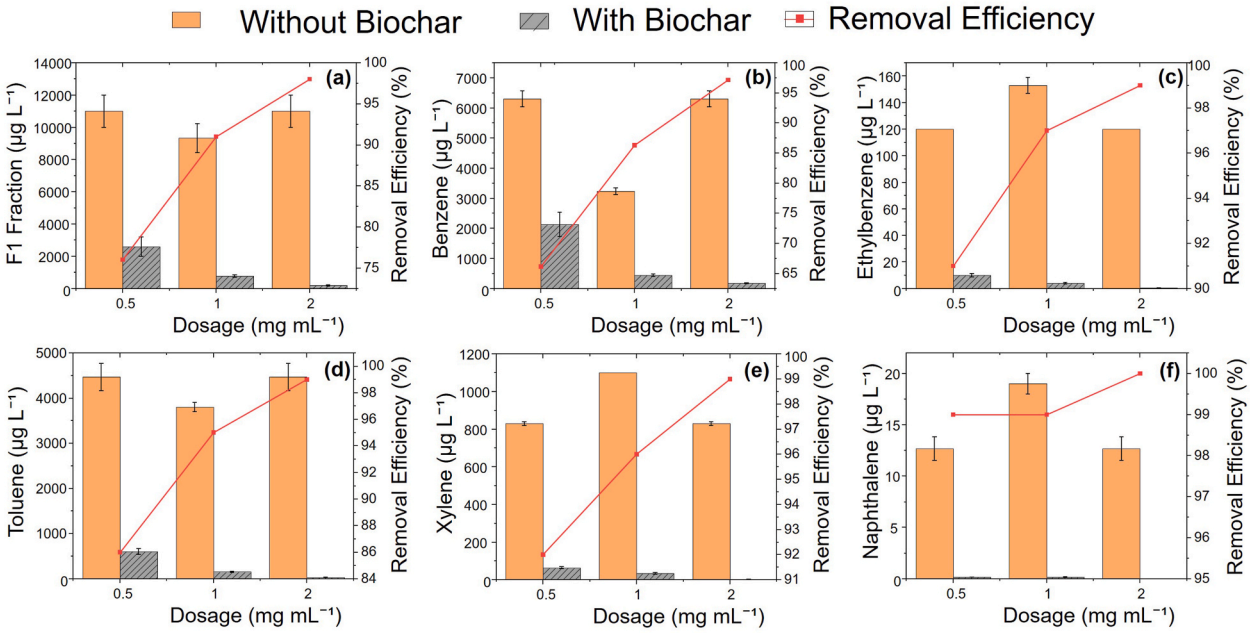

Fig. 4. Removal efficiency and contaminants concentration of petroleum hydrocarbons in ground water for various dosages of canola straw biochar. Comparative analysis of (a) F1, (b) benzene, (c) ethylbenzene, (d) toluene, (e) xylene, (f) naphthalene.
Note: The 1 g L^{-1} dosage data and the corresponding control without biochar were obtained from the primary kinetics experiment. The 0.5 g L^{-1} and 2 g L^{-1} experiments and their controls were conducted using separate, freshly spiked ground water batches, resulting in different initial concentrations. Removal efficiency calculations (Eq. (2)) are normalized to each batch's specific initial concentration, accounting for these differences.

the dosage increased to 2 mg mL^{-1} (Fig. 4d). Similarly, a low dosage of biochar (0.5 mg mL^{-1}) was effective in reducing xylene concentration by 92.4 %, with a removal efficiency of 99.6 % at 2 mg mL^{-1} (Fig. 4e).

This increase in removal efficiency with higher biochar dosage may be attributed to greater availability of diverse active sites on the biochar surface (Shen et al., 2024; Li et al., 2023). These sites interact with contaminants and absorb them on the surface. Hence, a higher biochar dosage indicates a greater number of active adsorption sites, thereby increasing removal efficiency. This finding aligns with the results of previous studies (Ali et al., 2020; Deng et al., 2021). From the XPS

analysis, the carbon content (C 1s) decreased from 70.09 to 65.04 %, suggesting surface coverage by PHCs or increased heteroatom signals (O, N). Higher dosages provide more carbon sites (sp^2/sp^3), thereby increasing adsorption capacity for F1–F2, BTEX, and PAHs through π-π and hydrophobic interactions.

Unlike the F1 hydrocarbons and the BTEX compounds, PAHs in the ground water were relatively independent of the biochar dosage. Most of the PAHs were almost entirely removed with the lowest dosage of biochar used. For example, with a 0.5 mg mL^{-1} biochar dosage, a 100 % removal efficiency was achieved for anthracene, acridine, fluorene, phenanthrene, 1-methylnaphthalene, and 2-methylnaphthalene. For naphthalene, 99 % removal efficiency was achieved at 0.5 and 1 mg mL^{-1}, and with an increase in dosage to 2 mg mL^{-1}, efficiency reached 100 % (Fig. 4f). A very high removal efficiency with a relatively small biochar dosage can be attributed to the low initial PAH concentrations in ground water. As a result, the active sites available at a lower biochar dosage were sufficient to adsorb them completely.

Increasing biochar dosage raises the number of available sorption sites and improves contact probability between contaminants and adsorbent, enhancing the likelihood of pore filling and multilayer adsorption (Murtaza et al., 2022). The observed plateauing of removal efficiency at higher dosages suggests limited contaminant access or competition for interior sites, consistent with previous findings for hydrocarbon and heavy metal adsorption. Biochar particle aggregation at excessive dosages can reduce effective surface area and mass transfer efficiency, as supported by studies showing that biochar aggregation is influenced by ionic strength and organic contaminant loading (Castan et al., 2019) Optimized biochar dosages from 1 to 10 g L^{-1} have been effective for hydrocarbon remediation in water systems (Alshahrani et al., 2022), with diminishing returns at excessive loadings due to aggregation or decreased mass transfer efficiency. The selected dosage (1 g L^{-1}) falls within this optimal range and demonstrates practical feasibility relative to higher-volume field applications, supporting the cost-effectiveness and scalability of this approach (Thompson et al., 2016). In contrast to studies that rely on ideal adsorbed solution theory (IAST) to predict competitive uptake, our empirical investigations in a real ground water matrix directly quantify the competitive adsorption effects of petroleum hydrocarbon mixtures.

Table 1
Fitting results of adsorption kinetic models for petroleum hydrocarbons removal using biochar.

Model	Contaminants	Model Parameters	R^2	F (p)	RMSE	AIC
Pseudo first order reaction	Benzene	$Q_e = 1164.287$; $K_1 = 0.008$	0.13	2.8 (0.12)	0.14	−49
	Toulene	$Q_e = 829.908$; $K_1 = 0.585$	0.81	42.8 (0)	0.34	−26
	Ethylbenzene	$Q_e = 11.274$; $K_1 = -0.004$	−0.11	0.1 (0.74)	0.58	−12
	Xylene	$Q_e = 120.937$; $K_1 = -0.005$	−0.05	0.5 (0.50)	0.38	−23
	F1 fraction	$Q_e = 913.398$; $K_1 = 0.002$	−0.08	0.1 (0.80)	0.42	−21
	F2 fraction	$Q_e = 8559.532$; $K_1 = -0.000$	0.18	1.7 (0.22)	0.34	−26
	1-MNAP	$Q_e = 1.145$; $K_1 = -0.015$	0.23	4.5 (0.06)	0.45	−19
	2-MNAP	$Q_e = 1.694$; $K_1 = -0.018$	0.21	4.2 (0.06)	0.53	−14
	NAP	$Q_e = 2.307$; $K_1 = -0.012$	0.22	3.7 (0.08)	0.36	−25
Pseudo second order	Benzene	$K_2 = 0.000066$; $Q_e = 3370$	0.99	883 (<0.01)	0	−145
	Toulene	$K_2 = -0.00047$; $Q_e = 3160$	0.99	2721 (<0.01)	0	−156
	Ethylbenzene	$K_2 = -0.0022$; $Q_e = 113.64$	0.98	822 (<0.01)	0.11	−56
	Xylene	$K_2 = -0.00033$; $Q_e = 87.40$	0.98	717 (<0.01)	0.02	−100
	F1 fraction	$K_2 = -0.00019$; $Q_e = 7870$	0.99	7571 (<0.01)	0	−186
	F2 fraction	$K_2 = -2.19$; $Q_e = 0.25$	0.99	11188 (<0.01)	13.11	46
	1-MNAP	$K_2 = -0.048$; $Q_e = 3.53$	0.98	733 (<0.01)	3.66	27
	2-MNAP	$K_2 = -0.041$; $Q_e = 3.82$	0.98	828 (<0.01)	3.18	24
	NAP	$K_2 = -0.013$; $Q_e = 12.67$	0.97	441 (<0.01)	1.31	1
Intraparticle diffusion	Benzene	$C = 2113.25$; $K_{id} = 2.52$	0.56	17.7 (0)	327.91	197
	Toulene	$C = 2432.88$; $K_{id} = 5.94$	0.37	8.6 (0.01)	426.61	204
	Ethylbenzene	$C = 127.06$; $K_{id} = 0.68$	−0.06	0.3 (0.60)	23.75	60
	Xylene	$C = 894.49$; $K_{id} = 3.23$	−0.07	0.1 (0.73)	172.08	172
	F1 fraction	$C = 6864.55$; $K_{id} = 101.52$	0.15	3.2 (0.10)	1069.94	240
	F2 fraction	$C = 0.42$; $K_{id} = -0.01$	0.24	5.1 (0.04)	1.52	8
	1-MNAP	$C = 9.62$; $K_{id} = -0.37$	0.62	22.5 (0)	1.47	7
	2-MNAP	$C = 15.07$; $K_{id} = -0.74$	0.7	31.5 (0)	2.49	17
	NAP	$C = 23.72$; $K_{id} = -0.52$	0.45	11.7 (0.01)	2.88	20
Elovich	Benzene	$\alpha = 7469356.34$; $\beta = 0.01$	0.76	38.1 (<0.01)	224.23	185
	Toulene	$\alpha = 6.98E{+}17$; $\beta = 0.02$	0.37	39.2 (<0.01)	227.82	185
	Ethylbenzene	$\alpha = 12547987242500$; $\beta = 0.23$	0.13	2.8 (0.12)	4.32	34
	Xylene	$\alpha = 4.98E{+}17$; $\beta = 0.04$	0.04	1.6 (0.24)	132.34	164
	F1 fraction	$\alpha = 962754432140$; $\beta = 0.00$	0.47	11.7 (0.01)	1128.51	242
	F2 fraction	$\alpha = -0.000000005$; $\beta = -36.13$	0.25	5.1 (0.05)	0.09	−61
	1-MNAP	$\alpha = -0.00004$; $\beta = -1.00$	0.72	32.2 (0)	1.24	−1
	2-MNAP	$\alpha = -0.0010$; $\beta = -0.48$	0.86	73.3 (<0.01)	1.72	11
	NAP	$\alpha = -0.000000004$; $\beta = -0.80$	0.46	11.1 (0.01)	2.62	18
Chemisorption and disffusion	Benzene	$Q_e = -1.46$; $K_{dc} = 0.0003$	0.97	390.0 (<0.01)	0.88	−6
	Toulene	$Q_e = -3.95$; $K_{dc} = 0.0003$	0.99	1154.8 (<0.01)	0.52	−15
	Ethylbenzene	$Q_e = 1.66$; $K_{dc} = 0.0087$	0.97	332.4 (<0.01)	0.95	−4
	Xylene	$Q_e = 1.61$; $K_{dc} = 0.0013$	0.96	316.0 (<0.01)	0.98	−3
	F1 fraction	$Q_e = -17.82$; $K_{dc} = 0.0001$	0.99	390.0 (<0.01)	0.88	−6
	F2 fraction	$Q_e = 1.48$; $K_{dc} = 4.09$	0.99	1653.4 (<0.01)	0.43	−20
	1-MNAP	$Q_e = 0.70$; $K_{dc} = 0.29$	0.96	305.7 (<0.01)	0.99	−3
	2-MNAP	$Q_e = 0.62$; $K_{dc} = 0.27$	0.96	305.4 (<0.01)	0.99	−3
	NAP	$Q_e = 0.79$; $K_{dc} = 0.08$	0.94	195.2 (<0.01)	1.23	−1

K1 = pseudo first order rate constant (min^{-1}); Q_e = amount of compound adsorbed at equilibrium (mg g^{-1}); K_2 = pseudo second order rate constant (g mg^{-1} min^{-1}); C = constant representing boundary layer effect; K_{id} = intraparticle diffusion rate constant (mg g^{-1} $min^{-0.5}$); α = initial rate of adsorption (mg g^{-1} min^{-1}); β = Elovich constant (g mg^{-1}); $K_{dc} = min^{-1}$; F1 = hydrocarbons with carbon chain lengths from C6 to C10; F2 = hydrocarbons with carbon chain lengths from C10 to C16; 1-MNAP = 1-methylnaphthalene; 2-MNAP = 2-methylnaphthalene; NAP = naphthalene; R^2 = coefficient of determination; F(p) = F-statistic (P-value); RMSE = root mean square error; AIC = akaike information criterion.

3.3. Adsorption kinetics of PHCs: chemisorption and diffusion-controlled mechanisms

Adsorption kinetics were evaluated using pseudo first order, pseudo second order, intraparticle diffusion, Elovich, and diffusion-chemisorption models (Table 1). Among the petroleum hydrocarbon contaminants, BTEX compounds, aliphatic fractions (F1, F2), and three PAHs (1-methylnaphthalene, 2-methylnaphthalene, naphthalene) demonstrated quantifiable kinetic behavior. The remaining PAHs could not be kinetically modeled because they were removed entirely immediately upon contact with the biochar. The pseudo second order model provided the best fit for most contaminants (Table 1), with adjusted R^2 values from 0.97 to 0.99 for BTEX compounds, 0.99 for F1 and F2 hydrocarbons, and 0.97–0.98 for the three PAHs. Similarly, the diffusion-chemisorption model exhibited strong correlations (Table 1), with adjusted R^2 values from 0.94 to 0.99 across all contaminants. The consistently high correlation coefficients (>0.94) for these two models indicate that the adsorption mechanism involves both chemical interactions and diffusion-controlled processes.

The adsorption of PHCs onto a biochar surface involves a complex mechanism that entails a multi-step process, incorporating both chemical interactions and diffusion between the PHCs and the biochar surface. The good fit of the pseudo-second-order model (Adjusted $R^2 >$ 0.97) suggests that the rate-limiting step may involve chemical interactions (chemisorption) between the pollutants and the biochar surface. This interpretation is supported by biochar surface analysis and by observed changes in surface functional groups from FTIR and XPS, while acknowledging that this model may also describe diffusion.

The multi-point BET analysis of biochar yielded a specific surface area of 89.12 m^2/g with a great fit to the BET model ($R^2 = 0.999964$). The high BET C constant (418.30) reflects strong adsorbate-adsorbent interactions, which are characteristic of microporous materials (Skic et al., 2024). CO_2 adsorption at 273 K (DFT analysis) yielded a surface area of 490.11 m^2/g, confirming that the biochar exhibits extensive ultramicroporosity (<0.7 nm). Nitrogen DFT analysis showed a bimodal pore distribution with a 1.54 nm mode and a 0.065 cm^3/g volume accessible. Complementary CO_2 DFT revealed additional ultramicropores (0.349 nm mode, 0.129 cm^3/g volume), providing high-energy sites for adsorption on theiochar surface (Chen et al., 2023). BJH analysis further confirmed mesopores (3.06 nm average diameter, 13.85 m^2/g surface area, 0.054 cm^3/g volume), which act as diffusion channels and multilayer adsorption sites for PHCs. Nitrogen isotherms showed type I/II behavior, indicating predominantly microporous structure with some mesopores, while the steep low-pressure uptake and gradual high-pressure rise reflect efficient micropore filling and mesopore condensation (Skic et al., 2024). CO_2 isotherms confirmed high-energy ultra-micropores, with the saturation volume corresponding to the measured micropore volume, supporting rapid adsorption kinetics consistent with pseudo-second-order behavior.

The FTIR analysis shows a weak and broad peak at 3050 cm^{-1} signifying aromatic C–H stretching, while the peak at 2900 cm^{-1} denotes aliphatic C–H stretching vibration. The medium intensity peak at 1587 cm^{-1} corresponds to aromatic C═C (Fig. 2). A medium-strong peak at 1457 cm^{-1} is attributed to aromatic ring vibrations and CH_2/CH_3 deformation. From the XPS C 1s spectra, a decrease in the aliphatic/aromatic C–H groups at 284 eV was observed for the biochar after adsorption. Two approximately equal peaks were observed at 284 eV prior to adsorption; however, after adsorption, one peak increased significantly, while the other decreased significantly (Fig. 3a–b). The increase of a particular peak at 284 eV could be because of the adsorption of linear PHCs (F1) on the biochar surface. These observations indicate the presence of graphitic domains in biochar and increased concentration of non-polar sites such as aliphatic or aromatic C–H groups, which serve as active sites for PHC adsorption. These active sites participate in chemical interactions, such as hydrophobic and π-π interactions, leading to adsorption of PHCs onto the biochar. Fitting to diffusion and chemisorption indicates that diffusion also contributes to the adsorption process (Obike et al., 2018; Huang et al., 2021). This dual-mechanism behavior demonstrates the heterogeneous nature of biochar surface interactions, where multiple active sites with varying accessibility and energy distributions facilitate contaminant uptake. For example, specific active sites on the biochar rapidly adsorb PHCs via chemisorption, while other sites located deeper may require additional time for PHC to access and interact with them (Xue et al., 2012). These assumptions could explain the adsorption process, as biochar has a distinctive physicochemical surface structure, characterized by functional groups and porosity.

3.4. Isotherm models of PHCs adsorption: remediation of PHCs through multilayer adsorption and surface interactions

Equilibrium adsorption behavior for BTEX compounds and F1 hydrocarbons was evaluated using eight isotherm models (Langmuir, Freundlich, Dubinin-Radushkevich, Halsey, Kiselev, Flory-Higgins, Temkin, and Jovanovic) (Table 2). At all tested concentrations, PAHs and F2 hydrocarbons were completely removed, leaving no equilibrium concentrations to allow isotherm model fitting. Hence, the adsorption data for these contaminants could not be fitted to the isotherm models considered.

Among the eight fitted isotherm models, the Freundlich, Halsey, and Temkin models exhibited superior predictive capability (Table 2, Supplementary Fig. 2). The Freundlich model showed the most consistent performance across all contaminants, with adjusted R^2 values of 0.98 (benzene), 0.96 (toluene), 0.95 (ethylbenzene), 0.91 (xylene), and 0.94 (F1). The Freundlich parameter (n_f) indicates the viability of the sorption process; n_f values greater than one promote adsorption (Chen and Yao, 2015). The n_f values for the adsorption of all BTEX and F1 hydrocarbons on biochar were 1.2–1.8. The Halsey model exhibited correlation coefficients identical to those of the Freundlich model, while the Temkin model achieved adjusted R^2 values from 0.85 to 0.99, with F1 hydrocarbons showing the highest correlation ($R^2 = 0.99$). A strong correlation with Freundlich and Halsey's model suggests that adsorption takes place on a heterogeneous surface, allowing for the potential of multilayer adsorption (Ayawei et al., 2017). A good fit to the Temkin model (B_T values: 0.63–42.37; K_T values: 0.11–55.58) indicates significant adsorbate-adsorbate interactions during the adsorption process.

It is important to acknowledge the limited reliability of the linearized Freundlich, Halsey, and Temkin isotherm results due to error structure distortion and biased parameter estimation. Therefore, to ensure the robustness and accuracy of parameter values, nonlinear fitting of these three models was performed (Table 3). The results demonstrated generally strong performance for PHCs but lower reliability for certain compounds. The Freundlich and Halsey models exhibited high coefficients of determination ($R^2 = 0.94$–0.98), low RMSE, and narrow 95 % confidence intervals for benzene, toluene, and xylene, indicating statistically robust fits. Parameter **A**, the Freundlich constant K_f or Halsey constant K_H, was large (≈258–358), reflecting high adsorption capacity and strong affinity of biochar toward aromatic hydrocarbons. Corresponding **B** values, adsorption intensity n_f and Halsey exponent n_H (≈0.5–0.7), denoted heterogeneous surface energies and multilayer adsorption, consistent with biochar's porous and chemically diverse surface. For the **Temkin model**, significant fits for benzene, toluene, and xylene ($R^2 \approx 0.95$–0.96, $p < 0.05$) produced moderate equilibrium binding constants K_T (0.1–0.7) and isotherm constants B_T (≈400–1100), indicating energetically favorable yet variable adsorption. In contrast, ethylbenzene and the aliphatic **F1** exhibited wide or negative confidence limits and non-significant p-values, suggesting limited model reliability.

The diverse functional groups and pores on the biochar surface create varying affinities for PHCs, causing them to adsorb unevenly across the surface (Deng et al., 2021). The multilayer adsorption mechanism is attributed to strong intermolecular forces, hydrophobic interactions, and variable binding energies that enable PHCs to form

Table 2
Fitting results of adsorption isotherm models for petroleum hydrocarbons removal using biochar.

Isotherm	Contaminants	Model Parameters	R^2	F(p)	RMSE	AIC
Langmuir	Benzene	q_m = 4.75E+04; K_l = 1.95E-02	0.91	40.2 (0.01)	0.01	−42
	Toluene	q_m = 2.57E+05; K_l = 8.16E-04	0.80	16.9 (0.03)	0	−55
	Ethylbenzene	q_m = 9.03E+03; K_l = -1.87E-01	0.84	21.5 (0.02)	0	−56
	Xylene	q_m = 8.46E+04; K_l = 3.51E-03	0.50	0.0 (0.77)	0.01	−41
	F1	q_m = 1.53E+05; K_l = 1.54E-03	0.77	14.2 (0.03)	0.01	−41
Freundlich	Benzene	n_f = 1.7984; K_f = 162.06	0.98	176.7 (0)	0.04	−26
	Toluene	n_f = 1.4502; K_f = 207.51	0.96	176.7 (0)	0.04	−26
	Ethylbenzene	n_f = 1.5630; K_f = 92.02	0.95	38.4 (0.10)	0.02	−20
	Xylene	n_f = 1.2311; K_f = 124.21	0.91	30.9 (0.03)	0.06	−19
	F1	n_f = 1.4823; K_f = 130.32	0.94	51.0 (0.02)	0.04	−22
D-R	Benzene	β = -43.01; Q_m = 2.55	0.74	12.3 (0.04)	0.32	−5
	Toluene	β = -3.91; Q_m = 7.09	0.74	12.4 (0.04)	0.37	−4
	Ethylbenzene	β = -0.12; Q_m = 5.17	0.81	9.4 (0.20)	0.11	−11
	Xylene	β = -1.84; Q_m = 2.32	0.95	58.8 (0.02)	0.10	−14
	F1	β = -2649.80; Q_m = 0.00	0.92	37.7 (0.03)	0.10	−14
Halsey	Benzene	n_H = -1.7984; K_H = 0.90	0.98	176.7 (0)	0.09	−18
	Toluene	n_H = -1.4502; K_H = 0.88	0.96	95.3 (0)	0.15	−13
	Ethylbenzene	n_H = -1.5630; K_H = 0.87	0.95	38.4 (0.10)	0.06	−15
	Xylene	n_H = -1.2311; K_H = 0.84	0.91	30.9 (0.03)	0.14	−12
	F1	n_H = -1.4823; K_H = 0.87	0.94	51.0 (0.02)	0.09	−15
Kiselev	Benzene	K_i = 0.0020; K_n = -14.14	0.86	25.0 (0.02)	0.01	−40
	Toluene	K_i = 0.0030; K_n = -55.49	0.52	5.4 (0.10)	0.07	−21
	Ethylbenzene	K_i = 0.0311; K_n = -58.18	0.95	42.4 (0.10)	0.09	−12
	Xylene	K_i = 0.0036; K_n = -34.28	−0.15	0.6 (0.52)	0.12	−13
	F1	K_i = 4.58E-04; K_n = -13.20	0.51	4.1 (0.18)	0	−48
Flory-Higgins	Benzene	n_{FH} = 4.3476; K_{FH} = 0.0102	−0.01	0.9 (0.40)	0.10	−17
	Toluene	n_{FH} = 51.7885; K_{FH} = 0.0079	0.04	1.1 (0.36)	0.20	−10
	Ethylbenzene	n_{FH} = 58.0499; K_{FH} = 0.0257	−0.21	0.7 (0.57)	0.06	−15
	Xylene	n_{FH} = 55.0925; K_{FH} = 0.0122	−0.43	0.6 (0.52)	0.12	−13
	F1	n_{FH} = 14.2462; K_{FH} = 0.0080	−0.05	0.8 (0.45)	0.11	−14
Temkin	Benzene	B_T = 2.3087; K_T = 0.1112	0.96	103.8 (0)	242.16	61
	Toluene	B_T = 2.2992; K_T = 0.3659	0.96	90.3 (0)	239.15	61
	Ethylbenzene	B_T = 42.3736; K_T = 5.1790	0.85	12.0 (0.18)	9.16	15
	Xylene	B_T = 6.1263; K_T = 0.7289	0.95	59.8 (0.02)	49.21	35
	F1	B_T = 0.6336; K_T = 55.5774	0.99	2895.9 (0)	68.89	38
Jovanovic	Benzene	K_J = 4.88E-04; Q_{max} = 583.11	0.90	38.0 (0.01)	0.20	−10
	Toluene	K_J = 6.02E-04; Q_{max} = 442.07	0.88	31.7 (0.01)	0.25	−8
	Ethylbenzene	K_J = 1.91E-02; Q_{max} = 12.71	0.86	26.3 (0.01)	0.31	−6
	Xylene	K_J = 2.98E-03; Q_{max} = 76.85	0.82	18.7 (0.02)	0.44	−3
	F1	K_J = 2.27E-04; Q_{max} = 1258.24	0.89	33.6 (0.01)	0.21	−9

$\mathbf{q_m}$ = monolayer coverage capacity (mg g^{-1}); $\mathbf{K_l}$ = Langmuir isotherm constant (L mg^{-1}); $\mathbf{K_f}$ = Freundlich isotherm constant ($mg^{1-(1/n)}$ $L^{1/n}$ g^{-1}); n_f = adsorption intensity; D-R = Dubinin-Radushkevich; β = Dubinin-Radushkevich isotherm constant related to the adsorption energy (mol ^{2}); $\mathbf{Q_m}$ = theoretical isotherm saturation capacity (mg g^{-1}); $\mathbf{K_H}$ = Halsey isotherm constant; $\mathbf{n_H}$ =Halsey equation exponents; $\mathbf{K_i}$ = Kiselev equilibrium constant (L mg^{-1}); $\mathbf{K_n}$ = constant of complex formation between adsorbed molecules; $\mathbf{K_{FH}}$ = Flory-Huggins equilibrium constant (L mg^{-1}); $\mathbf{n_{FH}}$ = model exponent; $\mathbf{K_T}$ = Temkin isotherm equilibrium binding constant (L mg^{-1}); B_T = Temkin isotherm constant; $\mathbf{K_j}$ = Jovanovic isotherm constant (L mg^{-1}); $\mathbf{Q_{max}}$ = maximum adsorption capacity in Jovanovic model (mg g^{-1}), F1 = hydrocarbons with carbon chain lengths from C6 to C10; R^2 = coefficient of determination; F(p) = F-statistic (P-value); RMSE = root nean square error; AIC = akaike information criterion.

successive layers beyond initial surface saturation. The aromatic nature of PHCs promotes π-π stacking interactions and hydrophobic associations, particularly as surface coverage increases (Yang et al., 2019). As the quantity of PHCs increases on a biochar surface, they enhance hydrophobic interactions, leading to formation of new layers. These attributes, along with the diverse surface characteristics of biochar, provide a range of binding energies that facilitate adsorption of PHCs at various sites, thereby creating layers. The integration of these PHCs across multiple layers, along with significant intermolecular pressures and hydrophobic contacts, may facilitate interactions among PHC molecules.

3.5. Surface functionalization effects on non-polar hydrocarbon remediation efficiency

This study primarily focuses on the adsorption of non-polar hydrocarbons (PAHs, F1–F3, BTEX) on biochar. However, the FTIR, XPS, and BET/CO_2 porosimetry analyses revealed important mechanistic insights into the biochar's interactions with the polar fractions of the PHCs and their potential impacts on non-polar petroleum hydrocarbons. The FTIR analysis shows a weak peak at 1795 cm^{-1} indicating the presence of C═O groups, likely from esters or ketones (Fig. 2). The presence of the –OH group could increase the biochar's hydrophilic properties, facilitating hydrogen bonding with PHCs and enhancing the adsorption of polar components in ground water (Chen and Chen, 2009). The high-resolution spectra showed that the oxygen content (O 1s) increased from 10.4 to 15.08 % after adsorption (Fig. 3), indicating adsorption of polar hydrocarbons and possible functionalization of the biochar surface (Ahmad et al., 2014). The notable increase in oxygen from 10.4 to 15.08 % creates discrete hydrophilic regions that effectively segregate and concentrate hydrophobic domains across the biochar surface (Fan et al., 2021). This spatial reorganization enhances the accessibility of non-polar compounds to hydrophobic adsorption sites (Fan et al., 2021), particularly benefiting larger PAH molecules that require specific geometric arrangements for effective π-π stacking interactions.

XPS analysis shows that potassium (K 2p) concentration decreased from 17.66 to 16.38 %, while calcium (Ca 2p) concentration increased significantly from 0.63 to 2.2 % (Fig. 5). Sodium (Na 1s) concentration decreased from 0.71 % before adsorption to undetected post-adsorption. The changes in Na, K, and Ca before and after adsorption suggest the possibility of ion change reactions on the biochar surface (Yuan et al., 2022). The increase in Ca ions on biochar can create a stronger, localized

Table 3
Non-liner fitting of results of Freundlich, Halsey, and Temkin isotherm model parameters for petroleum hydrocarbons removal using biochar.

Model	Pollutant	Parameter A				Parameter B				Adj.R2	Reduced $\chi 2$	p-value
		Value	SE	LCL	UCL	Value	SE	LCL	UCL			
Frendulich	Ethyl benzene	91.02	6.42	9.43	172	0.70	0.14	−1.07	2.47	0.94	93	0.053
	Benzene	258	70	33	482	0.47	0.05	0.32	0.62	0.98	57542	0
	Toluene	358	110	5	711	0.54	0.08	0.30	0.78	0.96	89732	0.001
	Xylene	146	41	−33	327	0.73	0.12	0.20	1.27	0.94	5518	0.006
	F1	204	99	−224	633	0.60	0.08	0.26	0.94	0.96	373352	0.004
Halsey	Ethyl benzene	91	6	9	172	0.70	0.14	−1.07	2.47	0.94	93	0.053
	Benzene	313	88	−65	693	0.44	0.05	0.23	0.65	0.97	47184	0.002
	Toluene	358	110	6	710	0.54	0.07	0.31	0.78	0.96	89732	0.001
	Xylene	146	41	−33	327	0.73	0.12	0.20	1.26	0.94	5518	0.006
	F1	204	98	−220	630	0.60	0.08	0.26	0.93	0.96	373352	0.004
Temkin	Ethyl benzene	5	2	−28	38	59	17	−158	277	0.85	252	0.179
	Benzene	0.11	0.03	0.01	0.21	1089	106	749	1429	0.96	97737	0.002
	Toluene	0.37	0.09	0.08	0.66	1094	115	727	1460	0.96	95317	0.002
	Xylene	0.73	0.15	0.08	1.38	410	53	182	639	0.95	4844	0.016
	F1	0.02	0	0.02	0.02	3970	74	3653	4287	0.99	9491	0

Parameter **A** represents the Freundlich constant K_f ($mg^{1-(1/n)} L^{1/n} g^{-1}$), Halsey constant K_H ($L\ mg^{-1}$), or Temkin equilibrium binding constant K_T ($L\ mg^{-1}$); depending on the model; Parameter **B** represents the Freundlich adsorption intensity n_f (dimensionless), Halsey exponent n_H (dimensionless), or Temkin isotherm constant B_T ($J\ mol^{-1}$ respectively; F1 = hydrocarbons with carbon chain lengths from C_6 to C_{10}; R^2 = coefficient of determination (dimensionless); p value = F-statistic (P-value); RMSE = root mean square error; AIC = akaike information criterion; UCL = upper confidence interval at 95 %; LCL = lower confidence interval at 95 %.

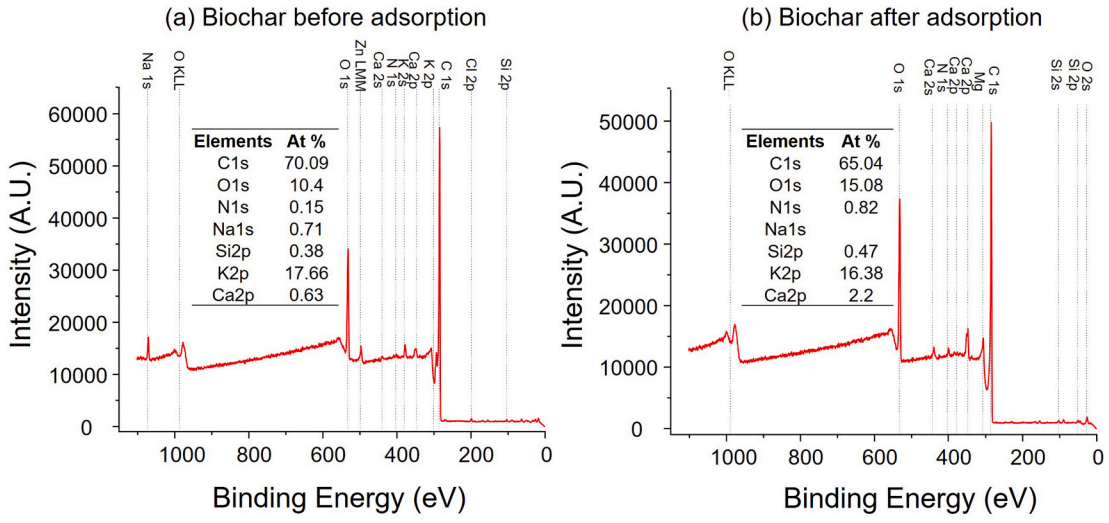

Fig. 5. X-ray photoelectron spectroscopy spectral analysis of biochar surface chemistry: changes in elemental composition and functional groups before and after petroleum hydrocarbon adsorption.

positive charge due to the divalent nature of Ca relative to monovalent ions such as K and Na. The resulting stronger electrostatic field helps stabilize the π-electron cloud and enhances-π interactions with aromatic hydrocarbons (Zhao et al., 2017). While XPS data provide valuable semi-quantitative insights into surface element trends during adsorption, complementary bulk analyses, such as ICP, should be included in future studies to more fully quantify the adsorption mechanisms. The biochar's hierarchical porosity enhanced adsorption by combining complementary porous structures. For example, ultra-micropores could provide high-energy sites for smaller compounds such as BTEX; micropores enabled additional BTEX adsorption; nd mesopores facilitated diffusion and multilayer adsorption, resulting in near-complete PAH removal (Gan et al., 2021).

This highlights the crucial role of ground water composition in PHC adsorption. Higher concentrations of divalent ions such as Ca^{2+} and Mg^{2+} in ground water (Table S3) potentially interact with biochar and influence the adsorption of non-polar PHCs onto its surface. Collectively, these changes demonstrate that PHC adsorption on biochar involves multiple mechanisms, including hydrophobic interactions and π-π stacking, with the latter being the primary mechanism driving adsorption. At the same time, hydrogen bonding and surface complexation facilitateadsorption of PHCs onto biochar by enhancing surface functionalization, thereby favouring adsorption.

3.6. Limitations of this study

Ground water collected from the site did not contain PHC concentrations above the guidelines and was therefore spiked with crude oil to simulate contamination. Although the same type of contamination source from the same site (crude oil) was used to replicate site conditions, this laboratory simulated contamination should not be equated with real-world contamination. While this study provides valuable insights, the results should be considered a starting point for field-based research rather than direct guidelines for remediation efforts.

The study does not account for the complex long-term weathering, aging, and microbial processes that occur under field conditions. Field contamination is inherently more complex than laboratory systems due to variable environmental dynamics and the natural aging of crude oil.

The isotherm analysis employed single-component models, which do not capture the complex competitive interactions among the 12 different hydrocarbons present in ground water. Due to the simultaneous presence of multiple petroleum hydrocarbon contaminants (BTEX, PAHs, F1–F2 hydrocarbons) in the crude oil-spiked ground water matrix, pure-component solutions were not available for individual isotherm determination. Consequently, multicomponent isotherm models that require single-component data, such as the Extended Langmuir or IAST models, could not be applied. Future work should employ these multicomponent approaches to better deconvolve competitive sorption effects among coexisting contaminants.

Activation energy validation for kinetic interpretation was not included in this study; incorporating such analysis in future work would help further refine mechanistic understanding. Similarly, full mass balance verification for potential volatile losses was not undertaken; while no major impacts on data interpretation are expected, additional verification steps could strengthen future assessments. Surface charge characterisation (e.g., zeta potential) was beyond the scope of this study, and its inclusion in subsequent work would provide deeper insight into the electrostatic interactions influencing adsorption.

The prolonged equilibrium times and high material dosages used in these batch tests were necessary to assess the material's maximum adsorption capacity. However, these specific parameters are not directly scalable for practical, continuous-flow applications where contact time and material economy are critical. This work, therefore, serves as a proof-of-concept and a foundational basis for future field-relevant studies.

4. Conclusions

Canola straw biochar was effective in reducing high concentrations of BTEX compounds and F1 hydrocarbons, while demonstrating the potential to completely remediate various PAHs and F2 hydrocarbons present in the ground water. The biochar's adsorption capacity was influenced by dosage and reaction time. While a lower dosage of canola straw biochar was sufficient for remediating PAHs and F2 hydrocarbons in ground water, a higher dosage enhanced the removal efficiencies of BTEX and F1 compounds, likely due to their higher initial concentrations. The kinetics and isotherm models, when combined with XPS and FTIR analysis, suggest that the adsorption process is multilayered on the heterogeneous surface of canola straw biochar and was primarily driven by chemisorption. This study provided insights into the functional groups involved in the adsorption process, which can help optimize biochar's properties for enhanced PHCs remediation. The hydrophobic sites on biochar surfaces served as primary active sites for PHC adsorption. Future research should validate these laboratory findings under true field conditions by conducting multicomponent adsorption experiments with petroleum hydrocarbon mixtures and dissolved organic matter to quantify competitive effects, evaluating long-term biochar performance under ground water aging, biofilm, and fouling scenarios, and performing pilot-scale tests in contaminated aquifers to bridge mechanistic insights and field-scale remediation.

CRediT authorship contribution statement

Abhijeet Pathy: Writing – review & editing, Writing – original draft, Visualization, Validation, Methodology, Investigation, Formal analysis, Data curation, Conceptualization. **M. Anne Naeth:** Writing – review & editing, Supervision, Software, Resources, Funding acquisition, Conceptualization. **Scott X. Chang:** Writing – review & editing.

Declaration of generative AI and AI-assisted technologies in the writing process

During the preparation of this work, the first author (Abhijeet Pathy) used Claude and ChatGPT to improve the sentence structure and readability of some of the content presented in the manuscript. After using Claude and ChatGPT, the author (Abhijeet Pathy) reviewed and edited the content as needed to fit his own writing style and takes full responsibility for the content of the published article.

Funding

This research was supported by Enbridge Pipelines and the University of Alberta. It was carried out as part of the University of Alberta's Future Energy Systems research initiative, funded in part by the Canada First Research Excellence Fund.

Declaration of competing interest

The authors declare that they have no known competing financial interests or personal relationships that could have appeared to influence the work reported in this paper.

Acknowledgements

The authors acknowledge Ms Sarah Wilkinson and Ms Stacy Campbell Court for their assistance with project administration and logistical support throughout the project. The authors acknowledge Mr. Henian Guo for his assistance with sample collection and laboratory experiments. The authors acknowledge Dr. Allen Jobson for his expert guidance in study design, field sampling techniques, and sample collection protocols.

Appendix A. Supplementary data

Supplementary data to this article can be found online at https://doi.org/10.1016/j.chemosphere.2025.144775.

Data availability

Data will be made available on request.

References

Oil Tanker Spill Statistics 2023 - ITOPF. https://www.itopf.org/knowledge-resources/data-statistics/statistics/. Accessed 18 December 2024.

Ahmad, M., Rajapaksha, A.U., Lim, J.E., Zhang, M., Bolan, N., Mohan, D., Vithanage, M., Lee, S.S., Ok, Y.S., 2014. Biochar as a sorbent for contaminant management in soil and water: a review. Chemosphere 99, 19–33. https://doi.org/10.1016/J.CHEMOSPHERE.2013.10.071.

Alexandersson, G., Klevebring, B., 2019. World resources-Energy, Metals, Minerals: Studies in Economic and Political Geography.

Ali, S., Rizwan, M., Shakoor, M.B., Jilani, A., Anjum, R., 2020. High sorption efficiency for As(III) and As(V) from aqueous solutions using novel almond shell biochar. Chemosphere 243, 125330. https://doi.org/10.1016/J.CHEMOSPHERE.2019.125330.

Alshahrani, F., Tawabini, B., Saleh, T., Alrayaan, M., Alaama, S., Nasser, R., Soupios, P., Kirmizakis, P., Mahmoud, M., Oyehan, T., Safi, E., 2022. Removal of benzene, MTBE and toluene from contaminated waters using biochar-based liquid activated carbon. Sci. Rep. 12. https://doi.org/10.1038/S41598-022-24283-6.

Ambaye, T.G., Chebbi, A., Formicola, F., Prasad, S., Gomez, F.H., Franzetti, A., Vaccari, M., 2022. Remediation of soil polluted with petroleum hydrocarbons and its reuse for agriculture: recent progress, challenges, and perspectives. Chemosphere 293, 133572. https://doi.org/10.1016/J.CHEMOSPHERE.2022.133572.

Ayawei, N., Ebelegi, A.N., Wankasi, D., 2017. Modelling and interpretation of adsorption isotherms. J. Chem., 3039817 https://doi.org/10.1155/2017/3039817, 2017.

Canadian Council of Ministers of the Environment (CCME), 2008. Canada-wide standard for petroleum hydrocarbons (PHC) in soil: User guidance (Version 1.1). PN 1398. https://ccme.ca/en/res/cws_phc_user_guide_1.1_e.pdf.

Castan, S., Sigmund, G., Hüffer, T., Hofmann, T., 2019. Biochar particle aggregation in soil pore water: the influence of ionic strength and interactions with pyrene. Environ Sci Process Impacts 21, 1722–1728. https://doi.org/10.1039/C9EM00277D.

Chen, B., Chen, Z., 2009. Sorption of naphthalene and 1-naphthol by biochars of orange peels with different pyrolytic temperatures. Chemosphere 76, 127–133. https://doi.org/10.1016/J.CHEMOSPHERE.2009.02.004.

Chen, X., Yao, M., 2015. Modeling of experimental adsorption isotherm data. Information 6, 14–22. https://doi.org/10.3390/INFO6010014, 2015, Vol 6, Pages 14-22.

Chen, S., Cai, H., Du, X., Wu, P., Tao, X., Zhou, J., Dang, Z., Lu, G., 2023. Adsorption behavior of hierarchical porous biochar from shrimp shell for tris(2-chloroethyl) phosphate (TCEP): sorption experiments and DFT calculations. Environ. Res. 219, 115128. https://doi.org/10.1016/J.ENVRES.2022.115128.

Deng, Y., Li, M., Zhang, Z., Liu, Q., Jiang, K., Tian, J., Zhang, Y., Ni, F., 2021. Comparative study on characteristics and mechanism of phosphate adsorption on Mg/Al modified biochar. J. Environ. Chem. Eng. 9, 105079. https://doi.org/10.1016/J.JECE.2021.105079.

Dong, M., He, L., Jiang, M., Zhu, Y., Wang, J., Gustave, W., Wang, S., Deng, Y., Zhang, X., Wang, Z., 2023. Biochar for the removal of emerging pollutants from aquatic systems: a review. Int. J. Environ. Res. Publ. Health 20, 1679. https://doi.org/10.3390/IJERPH20031679, 2023, Vol 20, Page 1679.

Fan, M., Li, C., Shao, Y., Zhang, S., Gholizadeh, M., Hu, X., 2021. Pyrolysis of cellulose: correlation of hydrophilicity with evolution of functionality of biochar. SSRN Electron. J. https://doi.org/10.2139/SSRN.3967428.

Fang, J., Wang, D., Wilkin, R., Su, C., 2025. Realistic and field scale applications of biochar for water remediation: a literature review. J Environ Manage 385, 125524. https://doi.org/10.1016/J.JENVMAN.2025.125524.

Gan, F., Cheng, B., Jin, Z., Dai, Z., Wang, B., Yang, L., Jiang, X., 2021. Hierarchical porous biochar from plant-based biomass through selectively removing lignin carbon from biochar for enhanced removal of toluene. Chemosphere 279, 130514. https://doi.org/10.1016/J.CHEMOSPHERE.2021.130514.

Ghodake, G.S., Shinde, S.K., Kadam, A.A., Saratale, R.G., Saratale, G.D., Kumar, M., Palem, R.R., AL-Shwaiman, H.A., Elgorban, A.M., Syed, A., Kim, D.Y., 2021. Review on biomass feedstocks, pyrolysis mechanism and physicochemical properties of biochar: State-of-the-art framework to speed up vision of circular bioeconomy. J. Clean. Prod. 297, 126645. https://doi.org/10.1016/J.JCLEPRO.2021.126645.

Gill, S., Gill, M., Ilyas, M.F., Farhad, M., Hannan, F., Lewińska, K., Virk, Z.A., Tauqeer, H. M., Ramzani, P.M.A., Iqbal, M., 2024. Current sources, fate, toxicity, governing factors, and remediation strategies for petrogenic hydrocarbons removal. Bio-organic Amendments for Heavy Metal Remediation: Water, Soil and Plant Approaches and Technologies 659–675. https://doi.org/10.1016/B978-0-443-21610-7.00032-X.

Guo, Y., Rockstraw, D.A., 2007. Activated carbons prepared from rice hull by one-step phosphoric acid activation. Microporous Mesoporous Mater. 100, 12–19. https://doi.org/10.1016/J.MICROMESO.2006.10.006.

Gupta, D.K., Gupta, C.K., Dubey, R., Fagodiya, R.K., Sharma, G., Keerthika, A., Mohamed, M.B.N., Dev, R., Shukla, A.K., 2020. Role of biochar in carbon sequestration and greenhouse gas mitigation. Biochar Applications in Agriculture and Environment Management 141–165. https://doi.org/10.1007/978-3-030-40997-5_7/FIGURES/8.

Gurav, R., Bhatia, S.K., Choi, T.R., Choi, Y.K., Kim, H.J., Song, H.S., Park, S.L., Lee, H.S., Lee, S.M., Choi, K.Y., Yang, Y.H., 2021. Adsorptive removal of crude petroleum oil from water using floating pinewood biochar decorated with coconut oil-derived fatty acids. Sci. Total Environ. 781, 146636. https://doi.org/10.1016/J.SCITOTENV.2021.146636.

Huang, J., Liu, F., Zhang, J., 2021. Insights into adsorption rate constants and rate laws of preset and arbitrary orders. Sep. Purif. Technol. 255, 117713. https://doi.org/10.1016/J.SEPPUR.2020.117713.

Islam, M.S., Kwak, J.H., Nzediegwu, C., Wang, S., Palansuriya, K., Kwon, E.E., Naeth, M. A., El-Din, M.G., Ok, Y.S., Chang, S.X., 2021. Biochar heavy metal removal in aqueous solution depends on feedstock type and pyrolysis purging gas. Environ. Pollut. 281, 117094. https://doi.org/10.1016/J.ENVPOL.2021.117094.

Kakkar, A., Kumar, S., Kumar, S., 2023. Remediation Technologies for Petroleum Hydrocarbons from the Environment, pp. 205–233. https://doi.org/10.1007/978-3-031-48220-5_10.

Kuppusamy, S., Maddela, N.R., Megharaj, M., Venkateswarlu, K., 2020. Regulatory Guidelines for total petroleum hydrocarbon contamination. Total Petroleum Hydrocarbons 207–224. https://doi.org/10.1007/978-3-030-24035-6_8.

Li, Y., Wang, B., Shang, H., Cao, Y., Yang, C., Hu, W., Feng, Y., Yu, Y., 2023. Influence of adsorption sites of biochar on its adsorption performance for sulfamethoxazole. Chemosphere 326, 138408. https://doi.org/10.1016/J.CHEMOSPHERE.2023.138408.

Logeshwaran, P., Megharaj, M., Chadalavada, S., Bowman, M., Naidu, R., 2018. Petroleum hydrocarbons (PH) in groundwater aquifers: an overview of environmental fate, toxicity, microbial degradation and risk-based remediation approaches. Environ. Technol. Innov. 10, 175–193. https://doi.org/10.1016/J.ETI.2018.02.001.

Mohammadi, L., Rahdar, A., Bazrafshan, E., Dahmardeh, H., Susan, M.A.B.H., Kyzas, G. Z., 2020. Petroleum hydrocarbon removal from wastewaters: a review, 2020 Processes 8. https://doi.org/10.3390/PR8040447. Page 447 8, 447.

Mohan, D., Sarswat, A., Ok, Y.S., Pittman, C.U., 2014. Organic and inorganic contaminants removal from water with biochar, a renewable, low cost and sustainable adsorbent – a critical review. Bioresour. Technol. 160, 191–202. https://doi.org/10.1016/J.BIORTECH.2014.01.120.

Mohanta, S., Pradhan, B., Behera, I.D., 2024. Impact and remediation of petroleum hydrocarbon pollutants on agricultural land: a review. Geomicrobiol. J. 41, 345–359. https://doi.org/10.1080/01490451.2023.2243925.

Murtaza, G., Ahmed, Z., Dai, D.Q., Iqbal, R., Bawazeer, S., Usman, M., Rizwan, M., Iqbal, J., Akram, M.I., Althubiani, A.S., Tariq, A., Ali, I., 2022. A review of mechanism and adsorption capacities of biochar-based engineered composites for removing aquatic pollutants from contaminated water. Front. Environ. Sci. 10, 1035865. https://doi.org/10.3389/FENVS.2022.1035865/FULL.

Obike, A., Igwe, J., Emeruwa, C., Uwakwe, K., Aghalibe, C., 2018. Diffusion-Chemisorption and pseudo-second order kinetic models for heavy metal removal from aqueous solutions using modified and unmodified oil palm fruit fibre. Chemical Science International Journal 23, 1–13. https://doi.org/10.9734/CSJI/2018/41459.

Ossai, I.C., Ahmed, A., Hassan, A., Hamid, F.S., 2020. Remediation of soil and water contaminated with petroleum hydrocarbon: a review. Environ. Technol. Innov. 17, 100526. https://doi.org/10.1016/J.ETI.2019.100526.

Shen, T., Peng, H., Yuan, X., Liang, Y., Liu, S., Wu, Z., Leng, L., Qin, P., 2024. Feature engineering for improved machine-learning-aided studying heavy metal adsorption on biochar. J Hazard Mater 466, 133442. https://doi.org/10.1016/J.JHAZMAT.2024.133442.

Skic, K., Adamczuk, A., Gryta, A., Boguta, P., Tóth, T., Jozefaciuk, G., 2024. Surface areas and adsorption energies of biochars estimated from nitrogen and water vapour adsorption isotherms. Sci. Rep. 14, 1–14. https://doi.org/10.1038/S41598-024-81030-9. SUBJMETA.

Speight, J.G., 2006. The chemistry and technology of petroleum. In: The Chemistry and Technology of Petroleum, fourth ed. https://doi.org/10.1201/9781420008388/CHEMISTRY-TECHNOLOGY-PETROLEUM-JAMES-SPEIGHT Fourth Edition 1–947.

Sun, X., Fu, H., Bao, M., Liu, W., Luo, C., Li, Y., Li, Y., Lu, J., 2022. Development of a new hydrophobic magnetic biochar for removing oil spills on the water surface. Biochar 4, 1–17. https://doi.org/10.1007/S42773-022-00184-9/FIGURES/10.

Thompson, K.A., Shimabuku, K.K., Kearns, J.P., Knappe, D.R.U., Summers, R.S., Cook, S. M., 2016. Environmental comparison of biochar and activated carbon for tertiary wastewater treatment. Environ. Sci. Technol. 50, 11253–11262. https://doi.org/10.1021/ACS.EST.6B03239.

U.S. Environmental Protection Agency (US EPA), 1996a. Method 8260D (SW-846): Volatile Organic Compounds by Gas Chromatography/Mass Spectrometry (GC/MS), Revision 4. U.S. Environmental Protection Agency. Environmental Protection Agency, Washington, DC. https://www.epa.gov/sites/default/files/2018-06/documents/method_8260d_update_vi_final_06-11-2018.pdf. Available at:

U.S. Environmental Protection Agency (US EPA), 1996b. Method 3510C (SW-846): Separatory Funnel Liquid-Liquid Extraction (Test Methods for Evaluating Solid Waste, Physical/Chemical Methods). U.S. Environmental Protection Agency, Washington, DC. https://www.epa.gov/sites/production/files/2015-12/documents/3510c.pdf. Available at:

U.S. Environmental Protection Agency (US EPA), 2018. Method 8270E (SW-846): Semivolatile organic compounds by gas chromatography/mass spectrometry (GC/MS). https://www.epa.gov/sites/default/files/2020-10/documents/method_8270e_update_vi_06-2018_0.pdf. Revision 6, June 2018. Washington, DC: U.S. EPA. Available at:

Wang, S., Xu, Y., Lin, Z., Zhang, J., Norbu, N., Liu, W., 2017. The harm of petroleum-polluted soil and its remediation research. AIP Conf. Proc. 1864. https://doi.org/10.1063/1.4993039/13750329/020222_1_ONLINE.PDF.

Xue, Y., Gao, B., Yao, Y., Inyang, M., Zhang, M., Zimmerman, A.R., Ro, K.S., 2012. Hydrogen peroxide modification enhances the ability of biochar (hydrochar) produced from hydrothermal carbonization of peanut hull to remove aqueous heavy metals: batch and column tests. Chem. Eng. J. 200–202, 673–680. https://doi.org/10.1016/J.CEJ.2012.06.116.

Yang, X., Li, Z., Liu, Y., Xing, Y., Wei, J., Yang, B., Zhang, C., Yang, R.T., Tsai, C.J., 2019. Research progress of gaseous polycyclic aromatic hydrocarbons purification by adsorption. Aerosol Air Qual. Res. 19, 911–924. https://doi.org/10.4209/AAQR.2018.11.0398.

Yuan, D., Zhang, L., Wan, S., Sun, L., 2022. Rational design of microporous biochar based on ion exchange using carboxyl as an anchor for high-efficiency capture of gaseous p-xylene. Sep. Purif. Technol. 286, 120402. https://doi.org/10.1016/J.SEPPUR.2021.120402.

Zhang, X., Zhao, B., Liu, H., Zhao, Y., Li, L., 2022. Effects of pyrolysis temperature on biochar's characteristics and speciation and environmental risks of heavy metals in sewage sludge biochars. Environ. Technol. Innov. 26, 102288. https://doi.org/10.1016/J.ETI.2022.102288.

Zhang, Q., Hu, Y., Jiao, J., Wang, S., 2024. The impact of Russia–Ukraine war on crude oil prices: an EMC framework. Humanit. Soc. Sci. Commun. 11 (1 11), 1–12. https://doi.org/10.1057/s41599-023-02526-9, 2024.

Zhao, Q., Zhang, S., Zhang, X., Lei, L., Ma, W., Ma, C., Song, L., Chen, J., Pan, B., Xing, B., 2017. Cation-Pi interaction: a key force for sorption of fluoroquinolone antibiotics on pyrogenic carbonaceous materials. Environ. Sci. Technol. 51, 13659–13667. https://doi.org/10.1021/ACS.EST.7B02317/ASSET/IMAGES/LARGE/ES-2017-02317J_0005.JPEG.